HHS Public Access

Author manuscript

J Proteomics. Author manuscript; available in PMC 2024 September 02.

Published in final edited form as:

J Proteomics. 2012 March 16; 75(6): 1838–1848. doi:10.1016/j.jprot.2011.12.025.

Proteomic changes at 8 weeks after infection are associated with chronic liver pathology in experimental schistosomiasis

Bhagyashree Manivannan[a], **T. William Jordan**[a], **W. Evan Secor**[b], **Anne Camille La Flamme**[a,*]

[a]Centre for Biodiscovery and School of Biological Sciences, Victoria University of Wellington, Wellington, 6140 New Zealand

[b]Division of Parasitic Diseases and Malaria, Centers for Disease Control and Prevention, Atlanta, GA, 30340, USA

Abstract

Chronic Schistosoma mansoni infection can present as a moderate or severe disease, termed intestinal or hepatosplenic schistosomiasis, respectively. Similarly, either moderate splenomegaly or hypersplenomegaly syndrome develops in CBA/J mice by 20 weeks of infection and is similar to intestinal or hepatosplenic schistosomiasis respectively. Using this mouse model and two-dimensional differential in gel electrophoresis, the liver proteomic signatures of uninfected mice and mice infected for 6, 8, 12, or 20 weeks were compared, and significant protein spots identified using mass spectrometry. We found the greatest number of changes at 12 weeks suggesting that this period represents the peak time of change. Pathway analysis identified specific proteins and pathways that correlated to the pathological changes indicative of severe disease, and these pathways were involved as early as 8 weeks after infection. These findings provide insight into the development of severe liver pathology in schistosomiasis and may aid in developing biomarkers for hepatosplenic schistosomiasis.

Keywords

Schistosomiasis; Hepatosplenic; Liver fibrosis; 2D-DIGE; Proteomics; MALDI-TOF/TOF

1. Introduction

Schistosoma mansoni infects almost 83 million people, causing intestinal schistosomiasis (INT) or hepatosplenic schistosomiasis (HS) in chronic infections [1]. *S. mansoni*-associated hepatosplenic disease is observed in 8.5 million people [2], and the clinical features include hypersplenomegaly, Symmers' fibrosis, portal hypertension, oesophageal varices and haematemesis, which may lead to death [3]. Our previous studies have evaluated the proteomics of schistosomiasis at 8 weeks of infection using C57BL/6 mice [4] and at 20 weeks of infection in CBA/J mice [5]. At 20 weeks after infection, the CBA/J mouse model

[*]*Corresponding author at:* School of Biological Sciences, Victoria University of Wellington, P.O. Box 600, Wellington, New Zealand. fax: +64 4 463 5331. anne.laflamme@vuw.ac.nz (A.C. La Flamme).

Appendix A. Supplementary

Supplementary data to this article can be found online at doi:10.1016/j.jprot.2011.12.025.

reflects the human chronic disease as hypersplenomegaly syndrome (HSS), observed in 20% of the infected mice, and is comparable pathologically and immunologically to HS. The remaining 80% of mice develop moderate splenomegaly syndrome (MSS), which is similar to INT [6]. Immunologically, these disease forms can be differentiated as early as 6 weeks after infection due to the development of cross-reactive idiotypes in MSS mice [7]. Because these distinct immunological differences can be identified early after egg laying begins, it is likely that other distinctive changes may be identified that can differentiate MSS from HSS earlier than 20 weeks of infection. Furthermore, these changes in combination with other markers of infection and immunity may have the potential to serve as diagnostic markers for severe disease.

We have previously demonstrated variations in the serum biomarkers cytokeratin 18, connective tissue growth factor and hydroxyproline during chronic schistosomiasis (MSS and HSS) [8]. The aim of this study was to identify differential protein abundance patterns associated with the segregation of the two chronic pathological forms. To that end, the proteomic signatures from the livers of CBA/J mice infected for 6, 8 and 12 weeks were compared with the abundance of proteins from 20 week infected animals as well as uninfected control mice using two-dimensional differential in gel electrophoresis (2D-DIGE) and MALDI MS/MS mass spectrometry. The protein spots that changed significantly were analysed using multivariate analysis and pathway analysis to assess the protein patterns and networks that may drive the chronic disease forms. We believe that the protein abundance studied at different time periods post-infection may help understand the molecular pathology of HSS and lead to the development of early diagnostic tools and more effective therapies for HS.

2. Materials and methods

2.1. Mouse liver sample collection

Male CBA/J mice were obtained from The Jackson Laboratory and were maintained at the American Association for Accreditation of Laboratory Animal Care, approved animal facility to the Centers for Disease Control and Prevention (CDC, Atlanta, USA) in accordance with institutional guidelines and federal regulations. The mice were infected by subcutaneous injection of 45 *S. mansoni* cercariae and liver samples were collected for uninfected control mice (n=5) and mice with 6 week (n=10), 8 week (n=10), 12 week (n=10) and 20 week (n=10) infections within the same time period and snap frozen at −80 °C. The 6, 8, and 12 week infected animals were randomly selected while the 20 week infected animals were selected based on their classification as having MSS or HSS (n=5 per group) upon necropsy [5]. Splenomegaly was expressed as percent spleen to body weight ratio (%SBW) and hepatomegaly expressed as percent liver to body weight ratio (%LBW). Two mice from each of the 8 and 12 week infection groups had noticeably higher %SBWs than other mice in the groups and thus were classified as pre-HSS (circled icons, Fig. 1A) and hence the infected mice from HSS (n=5), MSS (n=5), 12 week (n=8), 8 week (n=8) and mice with pre-HSS (n=4) were compared to uninfected control mice (n=5). All experiments performed were approved by Institutional Animal Care and Use Committee of the CDC as well as the The Victoria University of Wellington Animal Ethics Committee.

2.2. Liver total protein assay

Bio-Rad Protein Assay (Bio-Rad Laboratories, Life Science Group, USA) was used for mouse liver lysate total protein measurements (as per the manufacturer's guidelines).

2.3. Two-Dimensional Differential In Gel Electrophoresis

The liver lysate was subjected to 2D-DIGE using the Minimal CyDye Kit (GE Healthcare Bio-Sciences AB, Uppsala, Sweden) as per the manufacturer's guidelines. The experimental design is described in Table S1 of supplemental material. The sequentially scanned 2D-DIGE gel images were analysed using DeCyder™ 2-D (v 6.5, GE Healthcare). Data normalisation and statistical analyses were carried out using DeCyder software. The Biological Variation Analysis (BVA) module was used to match 69 gel images for pI ranges 4–7 and 6–11 each. The BVA compared the protein average volume ratios between study groups that changed by greater than 2-fold and one-way analysis of variance p value (1-ANOVA) ≤0.01 and passed the False Discovery Rate (FDR) feature; these spots were called 'protein spots of interest'. FDR feature eliminates false positive results, which are 1% of the significantly changed (1-ANOVA≤0.01) protein spots [9]. The Extended Data Analysis module was used for multivariate analyses which included the Principle Component Analysis (PCA) and Hierarchical Cluster Analysis (HCA) features as done previously [5]. We analysed the data in accordance for a target power of 0.8 [10]. The protein spot volume data for individual spots was extracted using the XML Toolbox module as described previously [11] to evaluate the mean and standard deviation measurements provided in Table S2 of the supplemental material.

2.4. Protein identification using mass spectrometry

Protein spots of interest were excised from preparative gels for tryptic digestion using an Ettan™ Digester (GE Healthcare). Tryptic digests were analysed using cyano-4-hydroxycinnamic acid (CHCA; Sigma-Aldrich) matrix and MALDI-TOF/TOF 5800 (Applied Biosystems, Foster City, CA) mass spectrometer operated in positive ion mode and continuous stage motion. Each spot was externally calibrated using TOF/TOF Calibration Mixture (Applied Biosystems), containing des-Arg^1-Bradykinin (m/z 905.05), Glu^1-Fibrinopeptide B (m/z 1571.61), angiotensin I (m/z 1297.51) and fragments of the adrenocorticotropic hormone 1–17 (m/z 2094.46), 18–39 (m/z 2466.72) and 7–36 (m/z 3660.19). MS spectra acquired over a mass range of 800–3500 m/z with a total of 400 laser shots/spectrum for each spot. A maximum of 21 precursors with S/N over 50 were selected for fragmentation. The MS/MS spectra were collected using air as the collision gas and were calibrated using angiotensin I fragmentation. For protein identification, all MS/MS data was submitted to Protein Pilot 3.0 software (Applied Biosystems) using MASCOT (v2.2.04, Matrix Sciences Ltd., UK) with IPI Mouse protein database v3.73 and search parameters as described previously [5]. The search results can be viewed at PRIDE (http://www.ebi.ac.uk/pride/) with accession numbers: 19316–19324.

2.5. Western blots

Liver lysate proteins from uninfected control and 6 week, 8 week, 12 week, 20 week infected mice were transblotted onto Hybond™-LFP membrane (GE Healthcare) and probed with antibodies for cytokeratin 18 and transferrin as described previously [5].

2.6. Pathway analysis

The DeCyder '2-fold change, 1-ANOVA≤0.01, with FDR' results and the Swiss/UniProt accession numbers of the identified protein spots were evaluated using MetaCore™ v6.7 (GeneGo, St. Joseph, MI, USA) specific for the liver organ and *Mus musculus* species. The MetaCore™ computes a score for each possible network according to the input protein list. The score is based on the hypergeometric distribution and is calculated with the right-tailed Fisher's Exact Test. The score is the negative logarithm to the base-10 of the Fisher's Exact Test p value that indicates the probability of the input protein list in a given network being found together as a result of random chance. The analysis generates a list of significant networks based on the input protein list. Top scored significant networks with high p-values are noted.

2.7. Statistical analysis

GraphPad Prism (v4.0, GraphPad, San. Diego, CA, USA) was used for normalisation and statistical analysis.

3. Results

3.1. Splenomegaly, hepatomegaly and disease kinetics

Splenomegaly (%SBW) and hepatomegaly (%LBW) are marked features of chronic schistosomiasis and reflect spleen and liver pathology during the disease. After log transformation of %SBW to normalise the data, comparison of the %SBW between the six study groups showed HSS mice were statistically different ($p \leq 0.0001$) from the other five groups (Fig. 1A). %LBW was elevated in all five groups compared to uninfected control mice (Fig. 1B). Linear regression analyses demonstrated significant correlations between %LBW and %SBW at 6, 8, 12 and 20 weeks of infection (Fig. 1C) during schistosomiasis.

Using the liver lysates, 2D-DIGE was performed to determine how the proteomic signatures altered over the course of schistosome infection. For the two pI ranges, the number of 'protein spots of interest' was 299 and 136 respectively. The highest number of changes compared to uninfected mice was observed in pre-HSS mice with 85 (pI 4–7) and 111 (pI 6–11) protein spots that had greater than 2-fold change in average volume ratio that were statistically different (1-ANOVA≤0.01) among the 5 infected groups (taken together) compared to uninfected control mice, and were not eliminated upon application of the DeCyder software FDR function. Of these 196 protein spots, mass spectrometry identified 127 protein spots (Fig. 2, Table 1 and Table S2 of supplemental material). The remaining 69 protein spots were relatively low in abundance and were not identified. Importantly, the highest number of changes compared to uninfected mice was observed for pre-HSS mice, followed by 12 week infected mice, with a total of 110 spots in both pI ranges that had

a greater than 2-fold change and 1-ANOVA≤0.01. Of these, 82 spots decreased while 28 protein spots increased in abundance (Fig. 1D).

To validate the protein spot data generated by 2D-DIGE, we assessed the protein abundance of two proteins (transferrin and cytokeratin) that showed distinct changes in abundance over the course of infection. Using linear regression analyses for cytokeratin 18 and transferrin 2D-DIGE spot volume data versus the western blot analysis band volume data, we found significant relationships between the two volumes (r^2=0.2647, p<0.001 and r^2=0.8494, p<0.001 respectively). Overall, this analysis indicated that similar results were generated from two independent experimental techniques involving the same samples (Figure S1 A, B of Supplementary material) thus supporting our use of spot volume data as a measure of protein abundance.

To further assess the disease-form specific changes, we compared the expression pattern of proteins that changed significantly in pre-HSS, MSS, and HSS mice. We found that 13 protein spots in pre-HSS and 10 protein spots in HSS mice were specific for those 2 groups (Table 2). No protein spots were exclusive to MSS mice. These results indicated that the pre-HSS protein spots may be predictive of pathology in the mice that follow the severe disease course. Moreover, the abundance of protein spots (n=60) shared by the pre-HSS and HSS mice suggests that the process that promotes severe disease pathology has already started in the pre-HSS mice.

3.2. Multivariate analysis

Multivariate analysis using principle components analysis (PCA) showed good separation of the study groups (each spot map represents the liver 2D-DIGE image for individual mice) for protein spots in pI range 4–7 (Fig. 3A). Uninfected control mice, 6 week infected mice, MSS and HSS mice demonstrated distinct clusters, with the 6 week infected mice clustered very closely to the uninfected controls. In contrast, while most 8 week and 12 week infected mice were clustered into distinct groups, the 8 week and 12 week mice that had been designated pre-HSS clustered with the HSS mice (Fig. 3A). Similar results were obtained for the pI 6–11 range PCA plot, but the clusters were less distinct because the proteins were more difficult to resolve on gels (data not shown). Overall, these results indicate that based upon proteomic signatures, the groups form distinct clusters, with the pre-HSS mice grouped with the HSS mice.

Unsupervised, hierarchical cluster analysis (HCA) segregated the study groups according to the individual disease status of each mouse based on proteins in the pI range 4–7 (Fig. 3B). The pre-HSS animals (wk0805, wk0809, wk1203 and wk1205) segregated with the HSS mice in the pI 4–7 dendrogram (Fig. 3B), supporting the conclusion that these mice were in the process of developing severe disease. The dendrogram for pI range 6–11 showed similar results but again the segregation of the groups was less clear due to the decreased resolution of those gels (data not shown). Taken together, this unsupervised HCA supports the findings of the supervised PCA analysis and indicates that the pre-HSS group is more similar to the HSS group than it is to other animals with the same length of infection.

3.3. Pathway analysis

To better understand how the changes we observed impacted liver pathology and processes, we used a web-based software tool, MetaCore™ for pathway analysis of the DeCyder data. The MetaCore™ pathway analysis showed the unique and common proteins between the different groups in our study. In the protein interaction networks, proteins (nodes) were pulled out from the original position to make visualisation, understanding and extracting information from the network easier. When the protein lists for 12 week infected mice, MSS, pre-HSS and HSS mice were compared, the analysis revealed 50 and 79 protein spots unique to HSS or pre-HSS mice, respectively in comparison to the MSS protein list (Fig. 4A, C). Further, 60 protein spots were shared by HSS and pre-HSS mice (Fig. 4B) and 51 protein spots were shared by 12 week infected and pre-HSS mice (Fig. 4D). These results again suggest that HSS and pre-HSS mice have a common protein set that relates to the development and pathology of schistosomiasis and reinforces the data presented in Table 1. MetaCore™ generated a list of networks for HSS (15 networks), pre-HSS (21 networks), MSS (5 networks), 12 week (17 networks) and 8 week (3 networks) mice protein spots. Of these, the top rated networks revealed similarities for HSS and pre-HSS mice proteins further supporting the supposition that pre-HSS mice were developing severe disease (Fig. 5 A, B). Additionally, the protein lists for MSS and the remaining 8 and 12 week infected mice had similar protein networks, suggesting that these mice were following a disease progression course similar to MSS mice (Figure S2 of supplemental material). The first top rated network for MSS mice (Figure S2A) was similar to the top rated network for 8 week (Figure S2B). The second top rated network for MSS mice (Figure S2C) was similar to the top rated network for 12 week infected mice (Figure S2D). Finally, comparison of the pre-HSS and HSS pathways revealed several shared core molecules: ESR1 (Estrogen receptor 1), c-Myc, p53 and c-Jun all of which are signalling proteins indicating that changes in these signalling pathways may be involved in the development of severe schistosomiasis.

4. Discussion

We aimed to study the early changes during the course of schistosomiasis infection associated with differential pathology in MSS and HSS by comparing the spleen and liver gross morphology and protein patterns at various time points post infection. Indeed, the %SBW comparison between the five study groups showed significant splenomegaly during severe schistosomiasis as previously indicated [6] with 20% of mice at 8 week and 12 week post-infection demonstrating a high %SBW. Multivariate analysis using PCA successfully distinguished the study groups according to the disease pattern (Fig. 3A), results that were confirmed by HCA (Fig. 3B). The HCA dendrogram showed clustering of mice with similar %SBW. This provides evidence that mice with high %SBW ratios at 8 and 12 weeks of infection (i.e. pre-HSS mice) are in the process of developing hepatosplenic disease, suggesting that these are crucial time points after infection with respect to chronic pathology and that the changes can be detected early in the disease.

A total of 424 protein spots were differentially expressed among the six study groups analysed together. These changes may be useful markers to determine the segregation of the chronic infection pathologic forms (MSS and HSS). While most differences in comparison

to uninfected control mice were in pre-HSS infected mice (i.e. 196 total protein spots), we also found a high level of change in 12 week infected mice (110 protein spots) and HSS mice (82 protein spots). Although, the greatest numbers of changes occurred in pre-HSS mice (mice with high %SBW) after infection, the greatest magnitude of change occurred in 20 week HSS infected mice. Interestingly, the protein spots identified for the pre-HSS and 12 week infection reflect the extent of liver dysfunction and the severity of liver damage as the proteins related to amino acid metabolism (homogentisate 1, 2-dioxygenase), fatty acid metabolism (acetyl-CoA acetyltransferase 2), xenobiotic metabolism (catalase, carbonic anhydrase III, glutathione S-transferase Pi), energy metabolism (aldolase 2, electron transfer flavoprotein beta-subunit, glutamate dehydrogenase) and urea cycle (carbamoyl phosphate synthase, argininosuccinate synthetase) were decreased significantly.

A study in 8 week *S. mansoni* infected mice analysed the metabolic profiles and reported reduced levels of the tricarboxylic acid cycle intermediates, increased pyruvate levels, and impairment in amino acid metabolism and fatty acid metabolism [12]. Previous work from our group demonstrated liver dysfunction at 8 weeks of infection [4] and other investigators showed changes in the urinary NMR spectra of *S. mansoni* infected individuals related to energy metabolism and liver function [13], similar to the results in our study. Previous studies have shown that there is spontaneous and prominent immunomodulation of chronic schistosomiasis pathology at 12 weeks of infection [14], supporting the findings in our study and suggesting that immunomodulatory mechanisms may contribute to the pathology profile at 12 weeks. Our report on liver proteins in CBA/J mice is unique as it compared hepatic protein abundance at 6, 8, 12 and 20 weeks post-infection and showed that the response is varied at different times after infection. Taken together, the protein spot abundance data for 6, 8 and 12 week infections in comparison to MSS and HSS suggests that the most dramatic changes occurred in the livers of 12 week infected CBA/J mice, indicating that this time point may be critical with respect to whether down-regulation of egg-induced pathology occurs or not.

Pathway analysis showed the multifaceted nature of schistosomiasis, revealing the complex networks and core molecules that contribute to the development of the disease (Fig. 5). In particular, ESR1, which has been studied extensively in apoptotic pathways and implicated in cancer [15], was identified as a potential HSS and pre-HSS core molecule. Previous research has shown that discoveries made through mass spectrometry of the signalling molecule p53 resulted in improved detection, therapeutics and molecular medicine of acute myeloid leukaemia [16]. Like ESR1 and p53, c-Myc protein has also been studied as a therapeutic target since it is related to apoptosis and cancer [18]. Thus, similar approaches may be applicable to schistosomiasis for development of diagnostic tools and treatments. Further, c-Jun, which was one of the core molecules in MSS, 8 week and 12 week infected networks in our study, is a mediator of early gene expression related to cell growth, differentiation, stress and is also associated with fibroblast proliferation [17]. The findings in our study may provide insight into the pathways that drive severe chronic disease pathology. The molecules revealed by pathway analysis in the signalling pathways during schistosome infection provide potential leads to a better understanding of the development of hepatosplenic disease. Importantly, during chronic disease deposition of excess extracellular matrix results in hepatic fibrosis which may lead to severe

consequences. Using the information from the pathway analysis, potential genes and proteins related directly or indirectly to hepatic fibrosis can be investigated. This knowledge will not only benefit the evaluation and treatment of schistosomiasis fibrosis but also fibrosis related to other liver diseases.

5. Conclusion

Our proteomic study of the liver at different stages of the *S. mansoni* used several different but complementary approaches to investigate and describe complex differences in protein patterns and pathology. PCA and HCA revealed unique protein patterns that are specific for different manifestations of chronic pathology. Results from these studies support the segregation of infected mice into MSS and HSS as early as 8 weeks of infection. Although the precise mechanisms and molecular factors that drive the progression of severe liver pathology are unknown, our pathway analysis highlighted several core signalling pathways that may be involved, including p53, c-Myc, c-Jun and ESR. Future investigations focused on the role of these core molecules in schistosomiasis may reveal new diagnostic and therapeutic targets for hepatosplenic schistosomiasis.

Supplementary Material

Refer to Web version on PubMed Central for supplementary material.

Acknowledgements

We thank Dr. Pisana Rawson, Danyl McLauchlan (Victoria University of Wellington, New Zealand) and Pete Augostini (Centre for Disease Control and Prevention, USA) for advice and assistance. The findings and conclusions in this report are those of the authors and do not necessarily represent the views of the CDC.

Funding

This work was supported by funds from the Victoria University of Wellington Research Fund [26251//1496] and Wellington Medical Research Foundation [2008/152].

Abbreviations:

%LBW	Hepatomegaly expressed as percent liver to body weight ratio
%SBW	Splenomegaly expressed as percent spleen to body weight ratio
2D-DIGE	Two-dimensional differential in gel electrophoresis
FDR	False discovery rate
HCA	Hierarchical cluster analysis
HSS	Hypersplenomegaly syndrome
MSS	Moderate splenomegaly syndrome
PCA	Principle component analysis

REFERENCES

[1]. Crompton DWT. How much human helminthiasis is there in the world? J Parasitol 1999;85:397–403. [PubMed: 10386428]

[2]. Van der Werf MJ, De Vlas SJ, Brooker S, Looman CWN, Nagelkerke NJD, Habbema JDF, et al. Quantification of clinical morbidity associated with schistosome infection in sub-Saharan Africa. Acta Trop 2003;86:125–39. [PubMed: 12745133]

[3]. Freeman GL Jr, Montesano MA, Secor WE, Colley DG, Howard MJ, Bosshardt SC. Immunopathogenesis and immunoregulation in schistosomiasis. Distinct chronic pathologic syndromes in CBA/J mice. Ann N Y Acad Sci 1996;797:151–65. [PubMed: 8993359]

[4]. Harvie M, Jordan TW, LaFlamme AC. Differential liver protein expression during schistosomiasis. Infect Immun 2007;75:736–44. [PubMed: 17101652]

[5]. Manivannan B, Rawson P, Jordan TW, Secor WE, La Flamme AC. Differential patterns of liver proteins in experimental murine hepatosplenic schistosomiasis. Infect Immun 2010;78:618–28. [PubMed: 19933830]

[6]. Henderson GS, Nix NA, Montesano MA, Gold D, Freeman GL Jr, McCurley TL, et al. Two distinct pathological syndromes in male CBA/J inbred mice with chronic *Schistosoma mansoni* infections. Am J Pathol 1993;142:703–14. [PubMed: 8456934]

[7]. Montesano MA, Colley DG, Willard MT, Freeman GL Jr, Secor WE. Idiotypes expressed early in experimental *Schistosoma mansoni* infections predict clinical outcomes of chronic disease. J Exp Med 2002;195:1223–8. [PubMed: 11994428]

[8]. Manivannan B, Rawson P, Jordan TW, Karanja DMS, Mwinzi PNM, Secor WE, et al. Identification of cytokeratin-18 as a biomarker of mouse and human hepatosplenic schistosomiasis. Infect Immun 2011;79:2051–8. [PubMed: 21357724]

[9]. GEHealthcare. DeCyder 2D Software, Version 6.5 User Manual. 28–4010–06 AB ed: GE Healthcare, 2005.

[10]. Karp NA, Lilley KS. Maximising sensitivity for detecting changes in protein expression: Experimental design using minimal CyDyes. Proteomics 2005;5:3105–15. [PubMed: 16035117]

[11]. Beddek AJ, Rawson P, Peng L, Snell R, Lehnert K, Ward HE, et al. Profiling the metabolic proteome of bovine mammary tissue. Proteomics 2008;8:1502–15. [PubMed: 18383006]

[12]. Wang Y, Holmes E, Nicholson JK, Cloarec O, Chollet J, Tanner M, et al. Metabonomic investigations in mice infected with *Schistosoma mansoni*: An approach for biomarker identification. Proc Natl Acad Sci U S A 2004;101:12676–81. [PubMed: 15314235]

[13]. Balog CIA, Meissner A, Goraler S, Bladergroen MR, Vennervald BJ, Mayboroda OA, et al. Metabonomic investigation of human *Schistosoma mansoni* infection. Mol Biosyst 2011, doi: 10.1039/c0mb00262c.

[14]. Pelley RP, Ruffier JJ, Warren KS. Suppressive effect of a chronic helminth infection, *Schistosomiasis mansoni*, on the in vitro responses of spleen and lymph node cells to the T cell mitogens phytohemagglutinin and concanavalin A. Infect Immun 1976;13:1176–83. [PubMed: 1084329]

[15]. Stein RA, McDonnell DP. Estrogen-related receptor α as a therapeutic target in cancer. Endocr Relat Cancer 2006;13:S25–32. [PubMed: 17259555]

[16]. Anensen N, Haaland I, D'Santos C, Van Belle W, Gjertsen BT. Proteomics of p53 in diagnostics and therapy of acute myeloid leukemia. Curr Pharm Biotechnol 2006;7:199–207. [PubMed: 16789904]

[17]. Karin M, Liu Z, Zandi E. AP-1 function and regulation. Curr Opin Cell Biol 1997;9:240–6. [PubMed: 9069263]

[18]. Gustafson WC, Weiss WA. Myc proteins as therapeutic targets. Oncogene 2010;29:1249–59. [PubMed: 20101214]

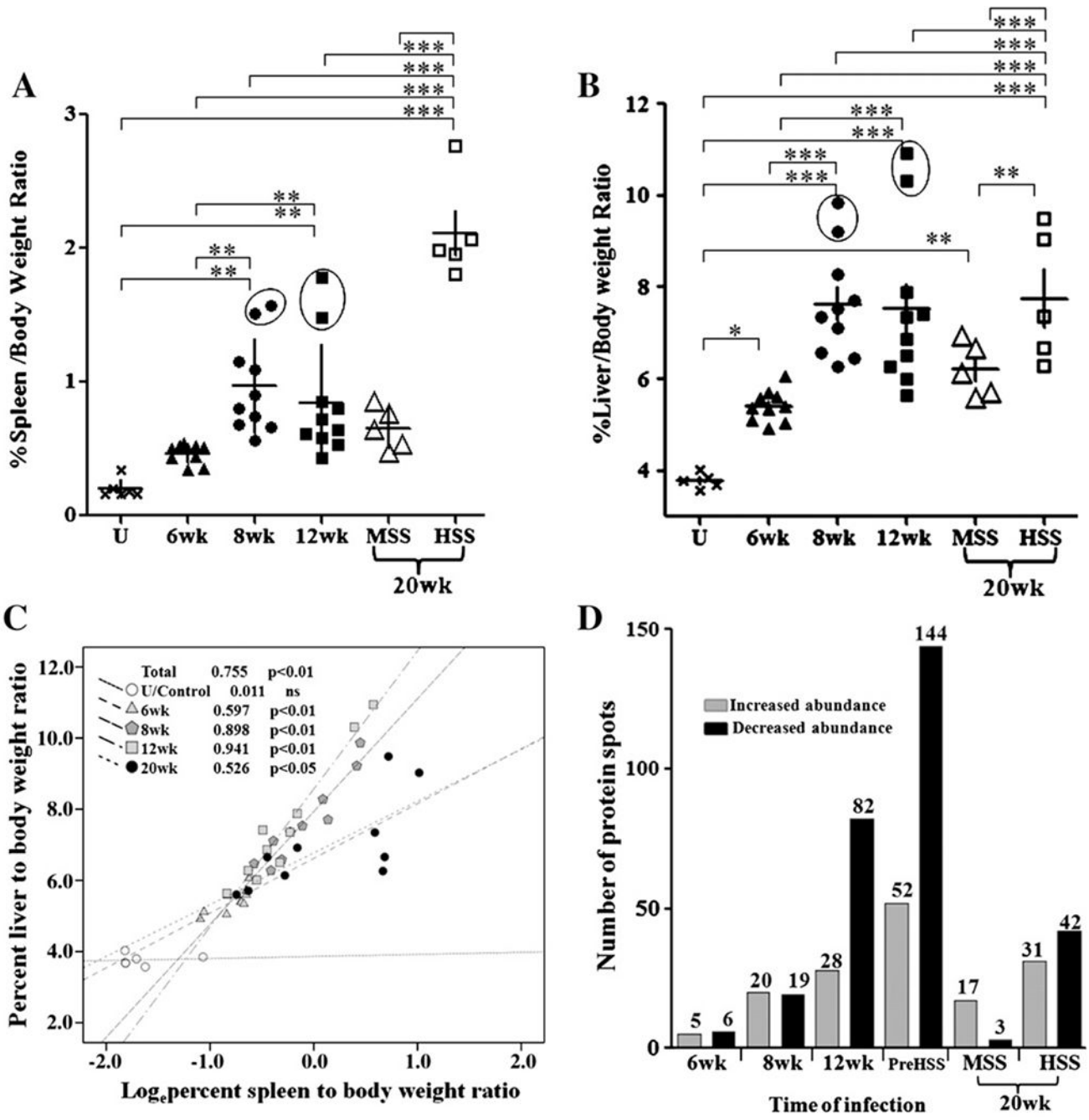

Fig. 1 –.

Comparison statistics between study groups A) Percent spleen to body weight ratio between six study groups. ***p≤0.001 when HSS mice were compared to uninfected control and 6 week, 8 week, 12 week infected mice and MSS mice; **p≤0.01 when 12 week, 8 week infected mice were compared to uninfected control and 6 week infected mice. Two mice from each of the 8 and 12 week infection groups (encircled) were classified as pre-HSS. Lines represent the mean±SEM. B) Percent liver to body weight ratio between six study groups. ***p≤0.001 when 8 week, 12 week, HSS mice were compared to uninfected control

mice and 6 week infected mice; **p≤0.01 when MSS were compared to HSS and uninfected control mice; *p≤0.05 when 6 week infected mice were compared to uninfected control mice. Lines represent the mean±SEM. C) Linear regression correlations and scatter plot for percent liver to body weight ratio and percent spleen to body weight ratio comparisons. D) Summary of protein spots that changed 2-fold, were statistically different (p≤0.01), and survived FDR for the five infected groups compared to uninfected control mice. (U=uninfected control, 6 wk=6 week infected, 8 wk=8 week infected, 12 wk=12 week infected mice, 20 wk=20 week infected mice (MSS and HSS)).

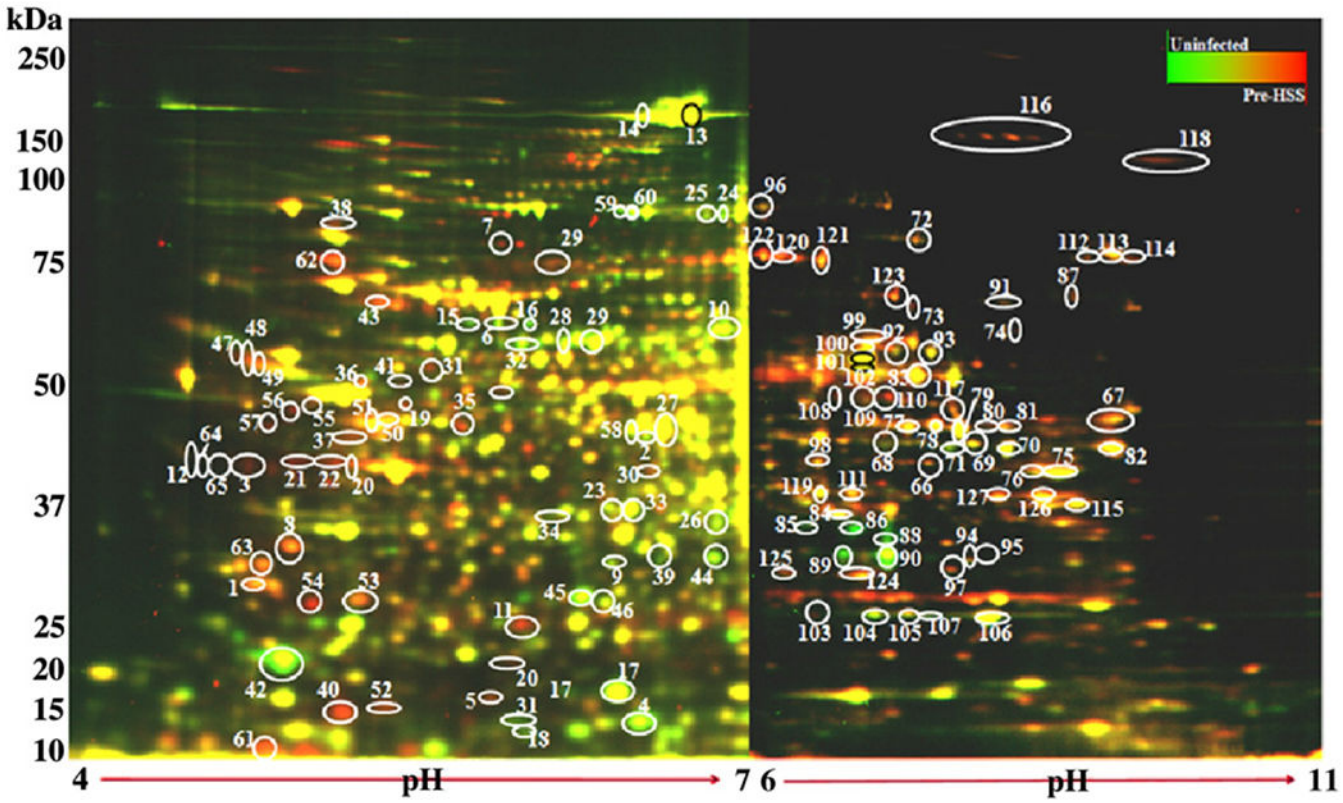

Fig. 2 –.

Liver proteomic signatures of 127 protein spots from uninfected control and pre-HSS mice using 2D-DIGE. Uninfected control liver lysate was labelled with Cy5 dye, Cy3 was used to label 20 week infected HSS liver lysate and Cy2 was used to label pooled internal standard (15 liver lysates from control uninfected, MSS and HSS mice, not shown). Proteins on IPG strips pI 4–7 and pI 6–11, 7 cm rehydrated overnight were isoelectric focussed and separated using SDS-PAGE. In the pseudocolor image protein spots present in both lysates appear yellow which is overlay of Cy5 and Cy3 images. Information on circled and numbered protein spots is given in Table 1 and Table S2 of supplemental material.

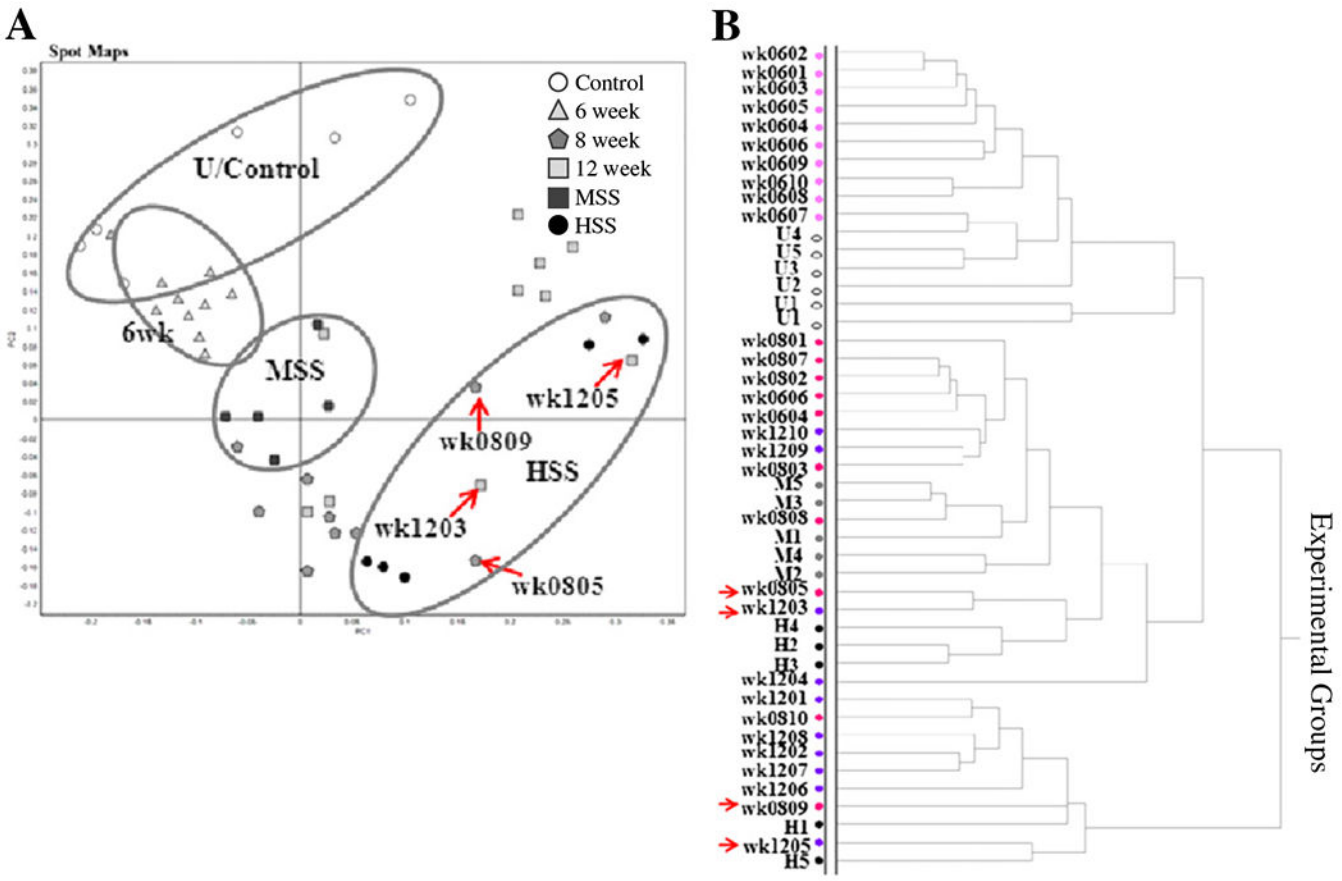

Fig. 3 –.

Multivariate analysis using 2D-DIGE data for pI range 4–7 with 2-fold change, 1-ANOVA≤0.01 and FDR for 41 protein spots. A) Principle component analysis plot spot maps (2D-DIGE images) show the best separation of the uninfected control and 6 week infected, MSS and HSS infected mice with 8 week infected and 12 week infected mice grouping with the 20 week infected mice (MSS and HSS) according to %SBW. B) Hierarchical cluster analysis showing dendrogram for the six study groups with the segregation and clustering of experimental groups with similar disease pathology. (U=uninfected control, wk0601-10=6 week infected, wk0801-10=8 week infected, wk1201-10=12 week infected, M=MSS, H=HSS). Red arrows indicate mice with high % spleen to body weight ratios.

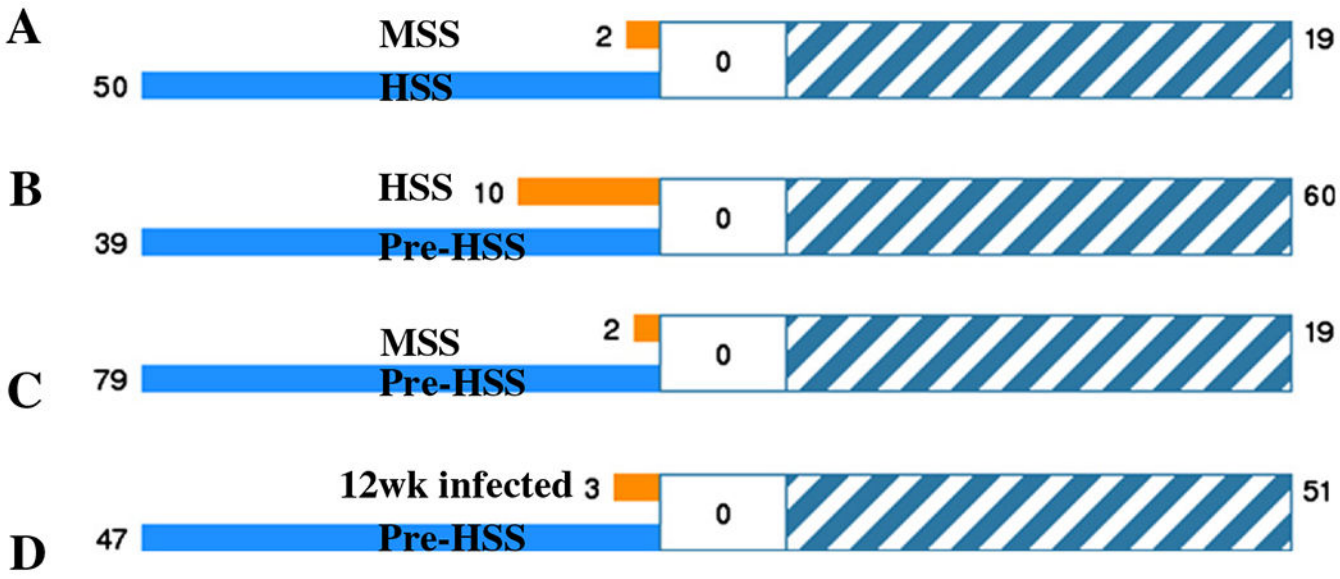

Fig. 4 –.

Pathway analysis using MetaCore™. List of 66 protein spots for 12 week infected mice, 11 for MSS mice, 97 for pre-HSS mice and 55 for HSS mice compared to uninfected control mice that were used for the pathway analysis. A) Comparison between MSS and HSS lists indicated that 14 protein spots are common while 44 protein spots are unique to HSS mice. B) Comparison between pre-HSS and HSS lists indicated 38 protein spots are common and 34 and 21 protein spots are unique to pre-HSS and HSS mice, respectively. C) Comparison between pre-HSS and MSS lists indicated 12 protein spots are common and 60 and 2 protein spots are unique to pre-HSS and MSS mice, respectively. D) Comparison between pre-HSS and 12 week infected mice lists indicated 26 protein spots are common and 13 and 30 protein spots are unique to 12 week infected mice and pre-HSS mice, respectively. The intersection set of experiments is defined as ‘common’ and marked as a striped bar. The unique genes for the experiments are marked as solid bars.

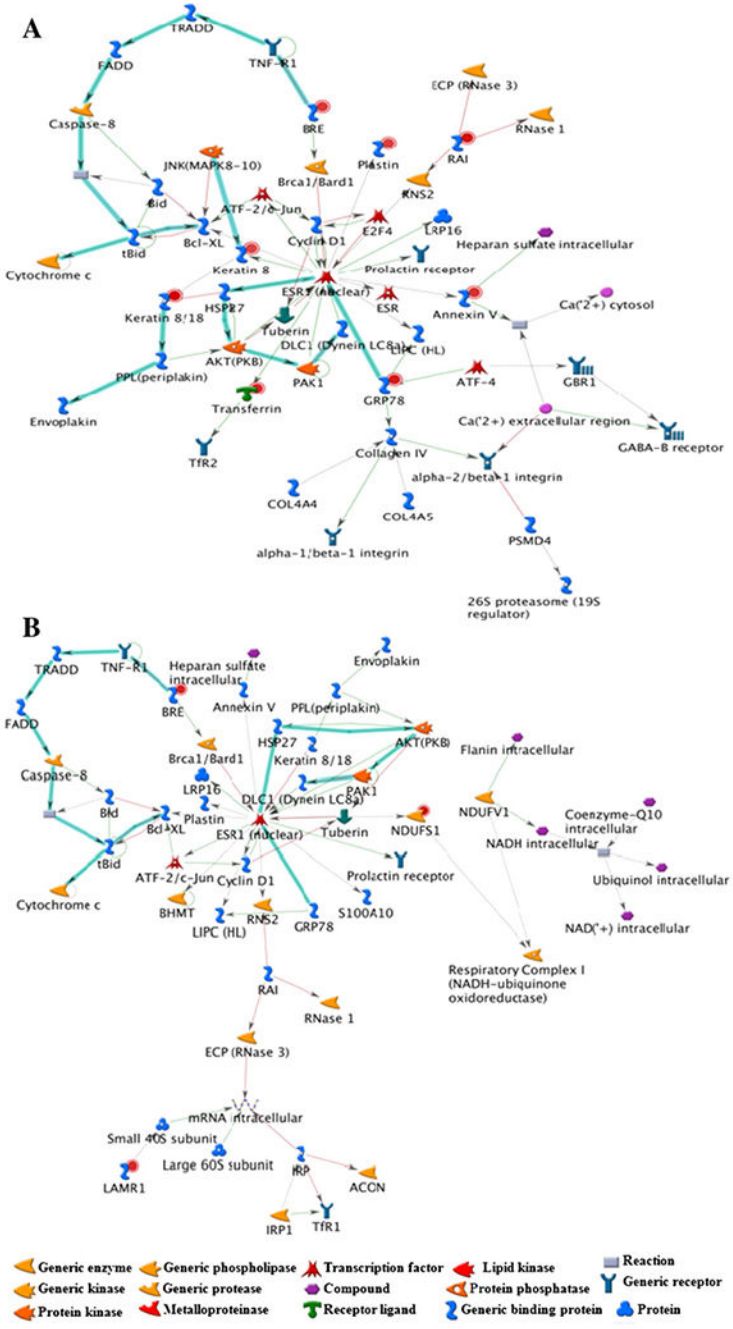

Fig. 5 –.

Networks generated for HSS and pre-HSS infected mice proteins using MetaCore™. A) The top rated HSS network had 8 protein spots. B) The pre-HSS network had 10 protein spots. The two networks A and B highlight important core molecule ESR1. According to the fold change data from our study the up-regulated genes are marked with red circles and the down-regulated with blue circles. The networks had $p<0.00001$. The key

to the most common network symbols is shown. Key to additional network symbols http://portal.genego.com/legends/network_legend.html.

Table 1 –

List of 127 protein spots for preHSS mice compared to uninfected control mice with≥2-fold change, 1-ANOVA≤0.01. Protein spots separated by 2D-DIGE were identified using MALDI-TOF/TOF mass spectrometry.

Spot No.	Protein name	UniProtKB /Swiss-Prot ID	AVR preH/U
1	14-3-3 Protein zeta/delta	P63101	+2.32
2	2-Oxoisovalerate dehydrogenase subunit alpha	P50136	−2.57
3	40S Ribosomal protein SA (laminin receptor 1)	P14206	+3.13
4	60S Ribosomal protein	P47963	−2.21
5	Actin-related protein 2/3 complex subunit 5	Q9CPW4	+3.71
6	Albumin	P07724	−3.28
7	Albumin 1	P07724	+3.57
8	Annexin 5	P48036	+3.16
9	Beta-lactamase-like protein 2	Q99KR3	−2.01
10	Bifunctional ATP-dependent dihydroxyacetone kinase	Q8VC30	−2.58
11	Brain and reproductive organ-expressed protein	Q8K3W0	+2.38
12	Calumenin	O35887	+2.70
13	Carbamoyl phosphate synthase	Q8C196	−3.67
14	Carbamoyl phosphate synthase	Q8C196	−4.17
15	Carboxylesterase 31-like	Q8VCU1	−2.26
16	Carboxylesterase 6	Q8QZR3	−2.37
17	Cu/Zn superoxide dismutase	P08228	−2.30
18	Cytochrome c oxidase subunit 5B; mitochondrial	Q9D881	−2.10
19	Cytokeratin 18	P05784	+2.56
20	Cytokeratin 18	P05784	+2.10
21	Cytokeratin 18	P05784	+3.10
22	Cytokeratin 18	P05784	+4.42
23	Dihydrodiol dehydrogenase	Q8K0E9	−2.01
24	Dimethylglycine dehydrogenase	Q5EBH4	−3.26
25	Dimethylglycine dehydrogenase	Q5EBH4	−3.12
26	Electron transfer flavoprotein subunit alpha	Q99LC5	−2.28
27	Enolase	Q5FW97	−2.60

Spot No.	Protein name	UniProtKB /Swiss-Prot ID	AVR preH/U
28	Epoxide hydrolase 2	P34914	−2.77
29	Epoxide hydrolase 2	P34914	−3.37
30	ER-associated Hsp40 co-chaperone	Q99KV1	+2.13
31	Fatty acid-binding protein; liver	P12710	−2.84
32	Formiminotransferase cyclodeaminase	Q91XD4	−2.86
33	Fructose-1,6-bisphosphatase 1	Q9QXD6	−2.06
34	Fructose-1,6-bisphosphatase 1	Q9QXD6	−2.31
35	Glutathione synthetase	P51855	+5.60
36	Guanine deaminase	Q69ZN0	+3.24
37	Heat shock 70 kDa protein	P20029	+3.29
38	Heat shock 90 kDa protein	Q71LX8	+4.46
39	Hydroxypyruvate isomerase homolog	A8Y5H8	−2.27
40	Interleukin-2	P70293	+4.64
41	Lymphocyte cytosolic protein 1	Q61233	+3.48
42	Major urinary protein 10	A2BIN1	−2.54
43	NADH dehydrogenase (ubiquinone) Fe-S protein 1	Q91VD9	+3.43
44	Omega-amidase NIT2	Q9JHW2	−2.09
45	Peroxiredoxin 6	O08709	−6.13
46	Peroxisomal-CoA diphosphatase	Q99P30	−2.12
47	Prolyl 4-hydroxylase; beta polypeptide	Q3UDR2	+3.64
48	Prolyl 4-hydroxylase; beta polypeptide	Q3UDR2	+3.53
49	Prolyl 4-hydroxylase; beta polypeptide	Q3UDR2	+2.60
50	Protein disulfide-isomerase A6	Q922R8	+2.72
51	Protein disulfide-isomerase A6	Q922R8	+2.28
52	Retinol binding protein 1	Q00915	+4.39
53	Rho GDP-dissociation inhibitor 1	Q99PT1	+3.12
54	Rho GDP-dissociation inhibitor 2	Q61599	+12.96
55	Ribonuclease/angiogenin inhibitor 1	Q91VI7	+4.40
56	Ribonuclease/angiogenin inhibitor 1	Q91VI7	+2.71
57	Ribonuclease/angiogenin inhibitor 1	Q91VI7	+4.27
58	S-Adenosylhomocysteine hydrolase	Q5M9P0	−2.29

Spot No.	Protein name	UniProtKB /Swiss-Prot ID	AVR preH/U
59	Sarcosine dehydrogenase	Q8BU72	−3.06
60	Sarcosine dehydrogenase	Q8BU72	−4.65
61	SH3 domain-binding glutamic acid rich-like protein3	Q91VW3	+16.26
62	Transglutaminase 2	P21981	+3.89
63	Tropomyosin 3	Q8C7C3	+2.86
64	Vimentin	P20152	+3.19
65	Vimentin	P20152	+3.06
66	Acetyl-CoA acyltransferase	Q99JY0	−2.06
67	Acetyl- CoA acetyltransferase 2	Q8CAY6	−2.89
68	Acetyl- CoA acyltransferase 2	Q8BWT1	−3.78
69	Acetyl- CoA acyltransferase 2	Q8BWT1	−3.68
70	Acetyl- CoA acyltransferase 2	Q8BWT1	−4.67
71	Acetyl- CoA acyltransferase 2	Q8BWT1	−5.96
72	Aconitate hydratase	P28271	−7.79
73	Acyl-CoA dehydrogenase, very long chain	P50544	−3.42
74	Aldehyde dehydrogenase family 4 member A1	Q8CHT0	−2.98
75	Aldolase 2; B isoform	Q91Y97	−4.84
76	Aldolase 2; B isoform	Q91Y97	−5.25
77	Argininosuccinate synthetase	P16460	−3.17
78	Argininosuccinate synthetase	P16460	−3.96
79	Argininosuccinate synthetase	P16460	−3.71
80	Argininosuccinate synthetase	P16460	−3.87
81	Argininosuccinate synthetase	P16460	−4.26
82	Aspartate aminotransferase precursor	P05202	−2.98
83	ATP synthase alpha subunit	D3Z6F5	−3.63
84	Betaine-homocysteine methyltransferase	O35490	−2.26
85	Betaine-homocysteine methyltransferase	O35490	−3.00
86	Betaine-homocysteine methyltransferase	O35490	−3.95
87	Calcium binding carrier protein (Slc25A13)	Q9QXX4	−3.43
88	Carbonic anhydrase III	P16015	−5.63
89	Carbonic anhydrase III	P16015	−5.69

Spot No.	Protein name	UniProtKB /Swiss-Prot ID	AVR preH/U
90	Carbonic anhydrase III	P16015	−5.80
91	Carnitine palmitoyltransferase 2	P52825	−2.85
92	Catalase	Q91XI2	−4.05
93	Catalase	Q91XI2	−3.42
94	Electron transfer flavoprotein beta-subunit	Q9DCW4	−2.87
95	Electron transfer flavoprotein beta-subunit	Q9DCW4	−3.10
96	Elongation factor 2	P58252	−3.09
97	Enoyl-CoA hydratase	Q8BH95	−3.54
98	Fumarylacetoacetate hydrolase	Q3TC72	−2.53
99	Glutamate dehydrogenase	P26443	−2.68
100	Glutamate dehydrogenase	P26443	−3.66
101	Glutamate dehydrogenase	P26443	−2.88
102	Glutamate dehydrogenase	P26443	−2.34
103	Glutathione S-transferase class Pi 1	P19157	−2.95
104	Glutathione S-transferase class Pi 1	P19157	−2.83
105	Glutathione S-transferase class Pi 1	P19157	−2.28
106	Glutathione S-transferase class Pi 1	P19157	−2.14
107	Glutathione S-transferase, Mu 1	P10649	−2.98
108	Homogentisate 1; 2-dioxygenase	Q7TPP2	−4.00
109	Homogentisate 1; 2-dioxygenase	Q7TPP2	−3.41
110	Homogentisate 1; 2-dioxygenase	Q7TPP2	−3.74
111	Hydroxyacid oxidase 1; liver	Q9WU19	−3.76
112	Hydroxyacyl-CoA dehydrogenase	Q8BMS1	−4.97
113	Hydroxyacyl-CoA dehydrogenase	Q8BMS1	−6.12
114	Hydroxyacyl-CoA dehydrogenase	Q8BMS1	−4.90
115	Malate dehydrogenase 2	P08249	−2.63
116	MHC Class 1 HLA	Q31152	+11.47
117	NADH dehydrogenase (ubiquinone) flavoprotein 1, 51 kDa	Q91YT0	−2.64
118	*Sm*-PEPCK	C4PYL1	+5.99
119	Thiosulfate sulfurtransferase	Q545S0	−3.76
120	Transferrin	Q921I1	−4.49

Spot No.	Protein name	UniProtKB /Swiss-Prot ID	AVR preH/U
121	Transferrin	Q921I1	−3.92
122	Transferrin	Q921I1	−2.89
123	Transketolase	P40142	−2.68
124	Triosephosphate isomerase	P17751	−2.37
125	Triosephosphate isomerase	P17751	−3.30
126	Urate oxidase	P25688	−2.11
127	Urate oxidase	P25688	−2.40

Additional protein identification data, means and standard deviations for individual protein spots are listed in supplementary Table S2 and in PRIDE database with accession numbers: 19316–19324.

Table 2 –

Protein spots specific for pre-HSS and HSS[a] with≥2-fold change, 1-ANOVA≤0.01.

No.	Protein spots specific for pre-HSS	AVR [b] PH/U [b]	Protein accession no.
1.	14-3-3 Protein zeta/delta	+2.32	P63101
2.	Calumenin	+2.70	O35887
3.	Carnitine palmitoyltransferase 2	−2.85	P52825
4.	Fumarylacetoacetate hydrolase	−2.53	Q3TC72
5.	Guanine deaminase	+3.24	Q69ZN0
6.	Malate dehydrogenase 2	−2.63	P08249
7.	Protein disulfide-isomerase A6	+2.72	Q922R8
8.	Protein disulfide-isomerase A6	+2.28	Q922R8
9.	Urate oxidase	−2.11	P25688
10.	Urate oxidase	−2.40	P25688
11.	Transferrin [c]	−4.49	Q921I1
12.	Transferrin [c]	−3.92	Q921I1
13.	Transferrin [c]	−2.89	Q921I1
	Protein spots specific for HSS	**H/U[b]**	**Protein Accession No.**
1.	Actin	+2.54	P63260
2.	Actin	+3.80	P60710
3.	Cytokeratin 8	+2.31	P11679
4.	Lactoylglutathione lyase	−2.05	O08709
5.	Major urinary protein 11 and 8	−2.98	P04938
6.	Haemoglobin	−2.62	Q9CY10
7.	Haemoglobin	−2.26	Q9CY10
8.	Transferrin [c]	+4.42	Q921I1
9.	Transferrin [c]	+2.74	Q921I1
10.	Transferrin [c]	+3.47	Q921I1

[a] All protein spots showed≥2-fold change and were significant by 1-ANOVA, p≤0.01 for pre-HSS (n=4) and HSS (n=5) when compared to uninfected mice and spots were identified using MALDI MS/MS.

[b] AVR: average volume ratio between study groups (U, uninfected control; PH, pre-HSS; H, HSS mice).

[c] Transferrin was found in both HSS and pre-HSS lists but showed opposite trends in abundance.